JOURNAL OF GEOPHYSICAL RESEARCH, VOL. 115, D12101, doi:10.1029/2009JD013370, 2010

Observed and modeled controls on precipitation $\delta^{18}O$ over Europe: From local temperature to the Northern Annular Mode

Robert D. Field[1]

Received 12 October 2009; revised 13 January 2010; accepted 21 January 2010; published 16 June 2010.

[1] Stable isotopes of oxygen and hydrogen are important paleoclimate indicators and can be obtained from many different natural archives in Europe such as tree rings and speleothems. In this study, a comparison was made of controls on European precipitation $\delta^{18}O$ between observations from the Global Network of Isotopes in Precipitation and from the NASA Goddard Institute for Space Studies ModelE general circulation model. In both observations and the general circulation model, the local temperature effect was identified and extended outside of Europe. This temperature control, in turn, was related to a North Atlantic Oscillation-like dipole but with centers of action different than standard NAO definitions. An examination of midtropospheric circulation controls showed that European $\delta^{18}O$ in fact reflects the hemisphere-wide teleconnections associated with the Northern Annular Mode. Seasonal differences were found in the strength of all controls on $\delta^{18}O$, with the annual controls being the combination of strong winter and weak summer controls. The weaker temperature effect in summer is well-known and has been universally attributed to the effects of continental moisture recycling, but the results of this study show that an additional factor is the reduced variability in summertime atmospheric circulation. The strong agreement between observed and modeled controls can help to improve interpretations of paleoclimatic archives of $\delta^{18}O$, particularly in terms of shifts in atmospheric circulation.

Citation: Field, R. D. (2010), Observed and modeled controls on precipitation $\delta^{18}O$ over Europe: From local temperature to the Northern Annular Mode, *J. Geophys. Res.*, *115*, D12101, doi:10.1029/2009JD013370.

1. Introduction

[2] Stable water isotopes provide a primary means of high-resolution paleoclimate reconstruction from terrestrial sources such as ice cores, tree cellulose, speleothems, and lake sediment carbonate [*Jones et al.*, 2009]. Across different proxy material, $\delta^{18}O$ composition is influenced strongly by precipitation [*Sonntag and Schoch-Fischer*, 1985; *Leng and Marshall*, 2004; *Lachniet*, 2009], and a better understanding of the controls on precipitation $\delta^{18}O$ can improve interpretation of natural $\delta^{18}O$ archives influenced by the hydrological cycle.

[3] Precipitation $\delta^{18}O$ has been collected by national agencies since the 1960s, with data pooled under the International Atomic Energy Agency (IAEA)'s Global Network of Isotopes in Precipitation (GNIP). The network is uniquely dense over central Europe, allowing for detailed analyses of controls on regional $\delta^{18}O$ over multiple decades. Pioneering studies of controls on European $\delta^{18}O$ focused on the positive correlation between precipitation $\delta^{18}O$ and local surface air temperature, known as the temperature effect [*Rozanski et al.*, 1992]. The $\delta^{18}O$ composition of precipitation, however, reflects the entire history of an air mass, and so will also be influenced by nonlocal effects such as changes in transport pathway, and ultimately, changes in atmospheric circulation [*Sonntag and Schoch-Fischer*, 1985; *Jouzel et al.*, 1997; *Araguas-Araguas et al.*, 2000]. Recently, the North Atlantic Oscillation (NAO) was found to have considerable influence on European precipitation $\delta^{18}O$ during winter, with the positive NAO phase being associated with less depleted precipitation $\delta^{18}O$ [*Baldini et al.*, 2008]. There were also considerable $\delta^{18}O$ signatures over Europe associated with the more general Northern Annular Mode (NAM), identified through analyses with isotopically equipped general circulation models [*Schmidt et al.*, 2007; *Yoshimura et al.*, 2008]. Indeed, given its dominance of the northern hemisphere climate, considerable effort has gone into reconstruction of the NAO, but this has been based largely on ice core $\delta^{18}O$ from Greenland [*Rogers et al.*, 1998; *Werner and Heimann*, 2002; *Vinther et al.*, 2003], or on nonisotopic proxies over Europe such as tree ring widths [*Cook et al.*, 2002], speleothem band counting [*Proctor et al.*, 2000], or combinations thereof [*Trouet et al.*, 2009]. Much of this non-ice core proxy material also contains a $\delta^{18}O$ record, providing a complementary source of reconstruction information [*McDermott*, 2004; *Saurer et al.*, 2008; *Lachniet*, 2009].

[4] The goal of this study was to better understand controls on European precipitation $\delta^{18}O$, motivated by an interest in improving interpretation of European $\delta^{18}O$ paleoclimate archives. There were three key differences from previous

[1]Department of Physics, University of Toronto, Toronto, Canada.

0148-0227/10/2009JD013370

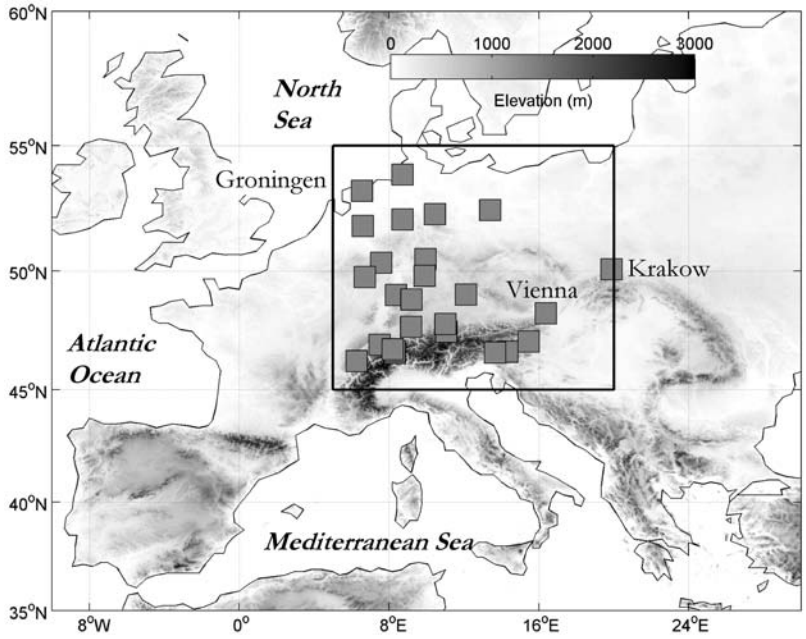

Figure 1. Map of GNIP stations used in the analysis, with labels for selected stations. The black rectangle shows the analysis domain.

analyses. Firstly, the differences in isotope-climate relationships between seasons were considered explicitly. Previous studies have focused on the season for which controls are expected to be strongest or on annual data [*Rozanski et al.*, 1992; *Vuille and Werner*, 2005]. Examination of seasonally selected data is useful in identifying the strongest controls, but not all isotopic archives are available with subannual resolution, and so it is important to understand what, if anything, controls δ^{18}O over all months of the year. Secondly, the spatial structure of controls on δ^{18}O was examined, for comparison to local temperature or predefined indices of circulation, such as those for the NAO, which may not in fact be the primary control of precipitation δ^{18}O over a given region. Lastly, any controls on European δ^{18}O identified in the GNIP observations were compared to those identified using an isotopically equipped general circulation model (GCM). GCMs have been successful in simulating the local temperature effect [*Hoffmann et al.*, 1998; *Cole et al.*, 1999; *Noone and Simmonds*, 2002; *Schmidt et al.*, 2007] and in identifying large-scale atmospheric circulation controls on precipitation δ^{18}O over Greenland and Antarctica [*Noone and Simmonds*, 2002; *Werner and Heimann*, 2002; *Schmidt et al.*, 2007] and over ice core sites at lower latitudes [*Vuille and Werner*, 2005]. Successful modeling of present-day δ^{18}O controls is the first step toward more mechanistic attribution of δ^{18}O variability to different causes during modern and preinstrumental conditions.

2. Data and Model Description

[5] Isotopic data were obtained from the publicly available GNIP data set [*IAEA*, 2001], consisting of monthly mean precipitation δ^{18}O data along with precipitation amount and temperature, collected since 1960. Compared to other areas in the world, the GNIP network is considerably more dense over central Europe, particularly over Germany, Austria, and Switzerland. Only stations with 20 or more years worth of data were included, similar to criteria used previously [*Rozanski et al.*, 1992]. There were 23 stations in the GNIP database that met these criteria, which represented half of all such stations in the GNIP database. Figure 1 shows the stations used in the analysis, with labels for selected stations.

[6] Relationships between δ^{18}O and climate were examined for individual stations and also for a regionally averaged European δ^{18}O record, following *Rozanski et al.* [1992]. To construct the regional average, precipitation δ^{18}O for reporting stations was interpolated linearly to a 1° × 1° grid each month, and a regional δ^{18}O mean was computed by weighting each grid cell by its interpolated precipitation amount. This way, the regional δ^{18}O estimate accounted for the uneven spatial distribution of stations, and also for variation in precipitation, to avoid bias toward drier locations, similar to temporal precipitation-weighting used in calculating seasonal means [*Vuille et al.*, 2003]. Confidence intervals (CIs) for all estimated parameters were computed at a 95% level using bootstrap resampling [*Efron and Gong*, 1983].

[7] The spatial structure of atmospheric circulation controls on regional δ^{18}O was identified by computing correlation maps from the National Centers for Environmental Prediction/National Center for Atmospheric Research Reanalysis [*Kalnay et al.*, 1996] for several meteorological fields at the surface and in the midtroposphere. Reanalysis data were available at a 2.5° × 2.5° horizontal resolution, with 17 vertical levels at standard pressure levels. This approach followed the observational analyses of circulation controls over Greenland δ^{18}O [*Rogers et al.*, 1998], Himalayan δ^{18}O [*Vuille et al.*, 2005], and western North American δ^{18}O [*Birks and Edwards*, 2009].

[8] These observational results were compared to those modeled using the NASA Goddard Institute for Space Studies ModelE GCM [*Schmidt et al.*, 2005], one of several GCMs

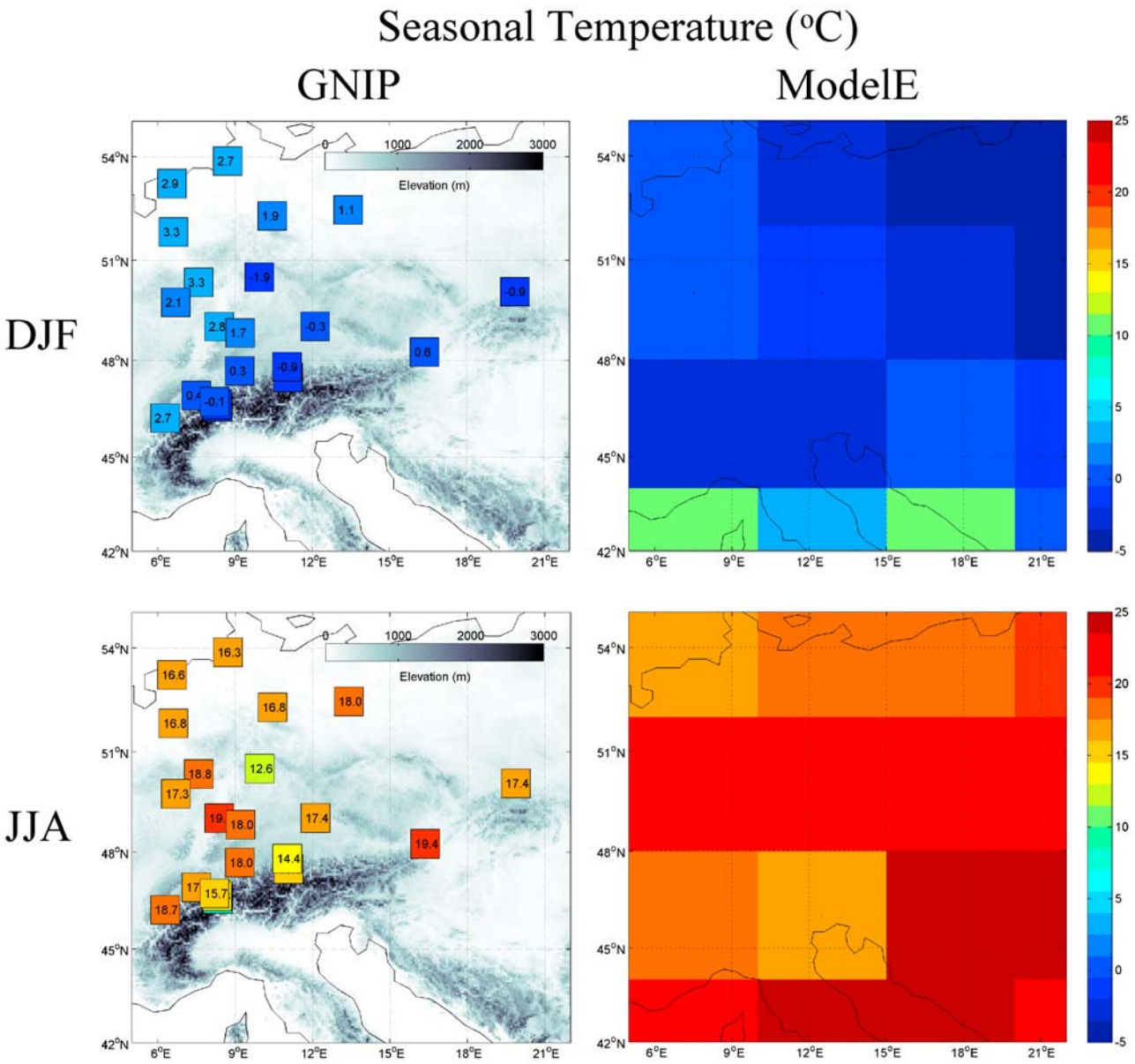

Figure 2. Seasonal temperatures (°C) at GNIP stations (left) and ModelE (right).

equipped with stable water isotope tracers. In the GCM, the fractionation between heavy and light isotopes is captured through all phases of the hydrological cycle, from evaporation over the ocean and land surface, to initial condensation and post-condensation exchange between condensate and vapor. The GCM has been shown to realistically simulate δ^{18}O seasonality over representative European GNIP stations and the main features of variability at a global scale [*Schmidt et al.*, 2005]. The model was run at a 4° × 5° horizontal resolution with 20 vertical levels for 45 years starting in 1954, forced with interannually varying sea surface temperature (SST) and sea-ice fields from the HadISST 1.1 data set [*Rayner et al.*, 2003] but with fixed greenhouse gas concentrations, similar to previous GCM studies [*Vuille et al.*, 2003]. The SSTs were prescribed from observations to induce realistic interannual variability, but a free-running, unnudged atmosphere produces a somewhat independent realization from the data-constrained reanalysis. This precludes direct comparison to observed δ^{18}O trends and interannual variability but guards against the results being overly sensitive to the choice of period analyzed.

3. Results

3.1. Mean Climatologies

[9] The GCM has been compared to observations at a global scale for basic climate diagnostics [*Schmidt et al.*, 2006] and isotopic quantities [*Schmidt et al.*, 2005]. Focusing more closely on Europe, we also compared spatial patterns of temperature, precipitation, and precipitation δ^{18}O. For temperature (Figure 2), there were slight continental and topographic gradients in the GNIP observations during December, January, and February (DJF), with cooler temperatures moving away from the North Sea eastward and into

Table 1. Regional Means for GNIP Observations and ModelE GCM[a]

	Months	Temperature (°C)		Precipitation (mm/d)		δ^{18}O (‰)		Years
GNIP	All	9.3	(8.7, 9.9)	2.2	(2.1, 2.3)	−9.1	(−9.3, −8.8)	37
	DJF	1.0	(0.5, 1.4)	1.9	(1.8, 2.1)	−11.5	(−11.9, −11.1)	36
	JJA	17.4	(17.2, 17.7)	2.7	(2.6, 2.9)	−7.0	(−7.2, −6.8)	39
ModelE	All	9.0	(8.3, 9.7)	1.8	(1.8, 1.9)	−8.6	(−8.9, −8.3)	45
	DJF	−1.3	(−1.7, −0.9)	1.8	(1.8, 1.9)	−12.6	(−12.8, −12.3)	45
	JJA	19.9	(19.6, 20.2)	1.8	(1.7, 1.9)	−4.6	(−4.8, −4.5)	45
Bias (ModelE-GNIP)	All	−0.3		−0.4		0.5		
	DJF	−2.3		−0.1		−1.1		
	JJA	2.5		−0.9		2.4		

[a]Values in parentheses are 95% confidence intervals.

the Alps. There was some indication of this cooling gradient in the GCM but with temperatures near the North Sea underestimated, which led to a cold bias of −2.3°C in the GCM during DJF across the domain (Table 1). Temperatures during June, July, and August (JJA) were generally overestimated in the GCM, with an average bias of 2.5°C across the domain. In both cases, this difference appeared to be statistically significant, given that the estimated GCM means fell outside the 95% CI of the GNIP mean and vice versa. The GCM tended, therefore, to overestimate the temperature seasonality observed in the GNIP data. In part, this reflects the paucity of observations in the eastern region of the domain which exhibited the greatest seasonality in the GCM.

[10] The main feature of the precipitation during both seasons is the increase from the northern European plain from rates of ~2 mm/d to values double that in the Alps (Figure 3). During DJF, there was a continental effect, with reduced precipitation moving inland from 1.9 mm/d at Groningen to a minimum value of 1.1 mm/d in Krakow. There was some indication of this continentality in the GCM and also of the increasing precipitation of up to 3.0 mm/d in the Alps and good agreement across the domain as a whole, with a bias of only −0.1 mm/d in the GCM (Table 1). On average, there were wetter conditions in JJA (2.7 mm/d), particularly in the Alps, which were not captured across the domain in the GCM (1.8 mm/d). There was some increase in precipitation in the northeast region of the domain, but the GCM failed to capture the magnitude of the JJA increase in the Alps.

[11] Like temperature, there were considerable spatial differences in precipitation δ^{18}O seasonality (Figure 4). The DJF values ranged from −8‰ in the coastal Netherlands to −13‰ in Krakow and −15‰ at the high Swiss alpine sites. In general, there was a sharp depleting effect with topography moving southward from the northern European plain to the Alps. These continental and orographic gradients during DJF were captured by the GCM but with the precipitation δ^{18}O overestimated near the coast in the northwest. Precipitation δ^{18}O was less depleted during JJA, particularly at the inland and the alpine stations, and with a more even spatial distribution. In Groningen, for example, the mean JJA δ^{18}O of −6.5‰ was 2.6‰ greater than the DJF value, compared to a JJA mean of −7.2‰ in Krakow, which was −5.8‰ greater than the DJF δ^{18}O. The GCM captured this seasonal difference but almost universally overestimated the JJA δ^{18}O, regardless of distance from the coast or elevation. Like temperature, the GCM tended to overestimate the seasonality of precipitation δ^{18}O, but this could be related to the paucity of GNIP data in the northeast region of the domain.

3.2. Local Temperature Controls on δ^{18}O

[12] Correlations between temperature anomalies and δ^{18}O anomalies are shown in Figure 5, at each station for the GNIP data, and in each grid cell for the GCM. There were significant differences for correlations computed separately for each season During DJF, the strongest correlation in GNIP data of $r = 0.63$ was at Vienna, with a median of $r = 0.38$ across all stations, and six stations with correlations of $r \geq 0.50$. There was also a general, if uneven, tendency toward a stronger temperature effect moving inland from the coast, which was better captured by the GCM compared to when all months were considered (not shown). Correlations weakened during JJA, with maximum correlation of $r = 0.50$ and median across stations of $r = 0.27$. The greatest decrease in correlation with temperature occurred over the Netherlands and Germany, but there were persistent positive correlations in Vienna and Krakow to the east, and over the Alps to the south, the latter pattern being fairly well represented in the GCM.

3.3. Spatial Temperature Controls on European δ^{18}O

[13] The high density of GNIP stations over central Europe allowed for the analysis of the relationships between δ^{18}O and temperature computed from regional averaging, in addition to temperatures outside of Europe. Figure 6 shows the linear relationship between the European δ^{18}O and temperature anomalies. Like the individual station correlations, these regional relationships were dependent on season, with a stronger correlation during DJF ($r = 0.56$) than JJA ($r = 0.39$). Whereas each seasonal correlation fell outside of the other's 95% CI, this was not the case for the regression slopes, which would not be considered statistically distinct.

[14] Precipitation δ^{18}O reflects the entire history of the air parcel from which the moisture originated and, in particular, the proportion of original moisture that rained out during transit. This will in part be determined by cooling during sloped, cyclonic ascent, and therefore the temperature along the air parcel's entire trajectory. To determine if the temperature correlation extended outside of the Europe domain, correlation maps were constructed between average European δ^{18}O and cell-by-cell surface temperature anomalies for the observations and GCM (Figure 7). During DJF, there is strong positive correlation west of the analysis region with southwest to northeast orientation, with that in the observations extending further southward and that in the GCM more

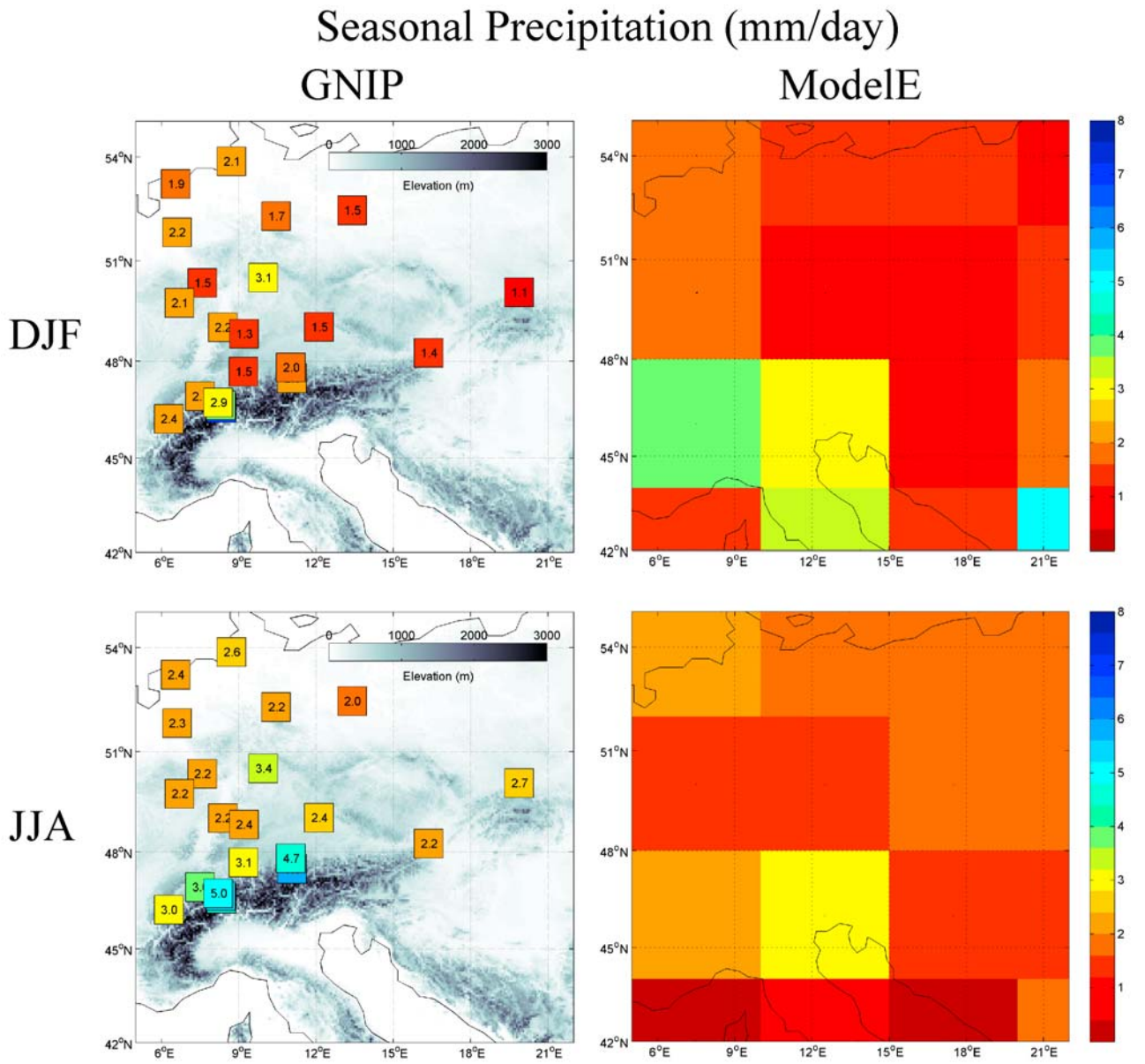

Figure 3. Seasonal precipitation (mm/d) at GNIP stations (left) and ModelE (right).

northward. At their strongest, the maximum values in the correlation field are stronger than those for strictly European temperature for both the observations ($r = 0.67$ compared to $r = 0.57$) and particularly for the GCM ($r = 0.74$ compared to $r = 0.58$). In the case of the observations, this could partly be a function of the more heavily assimilated nature of the Reanalysis data compared to the simple temperature averaging across GNIP stations. But for the GCM, the temperature fields used for the local and regional GCM correlations are the same, and so the stronger regional correlation likely indicates a stronger, physical upstream influence.

[15] The center of positive temperature correlation over Europe formed the northern center of a dipole, with a corresponding center of negative correlation over eastern North Africa. The strength of this negative pole was surprisingly strong in the observations ($r = -0.63$), nearly as strong as the main center of positive correlation. There were also secondary centers of negative correlation over Greenland and positive correlation over Siberia and the west Pacific, which were weaker in magnitude but robust in their spatial coherence.

[16] During JJA, the regions of positive correlations had contracted and were weaker at their strongest point. These maximum JJA correlations in the spatial field were still stronger, however, than the JJA correlations between European δ^{18}O and temperature strictly over Europe, with maxima of $r = 0.51$ in the observations and $r = 0.63$ in the GCM. The centers of negative correlation have also weakened and contracted during JJA, and the northern pole has also shifted eastward, with good agreement in these changes between GNIP and the GCM. Annual maps were also constructed (not shown) and, as might be expected, appeared as weakened versions of the DJF maps.

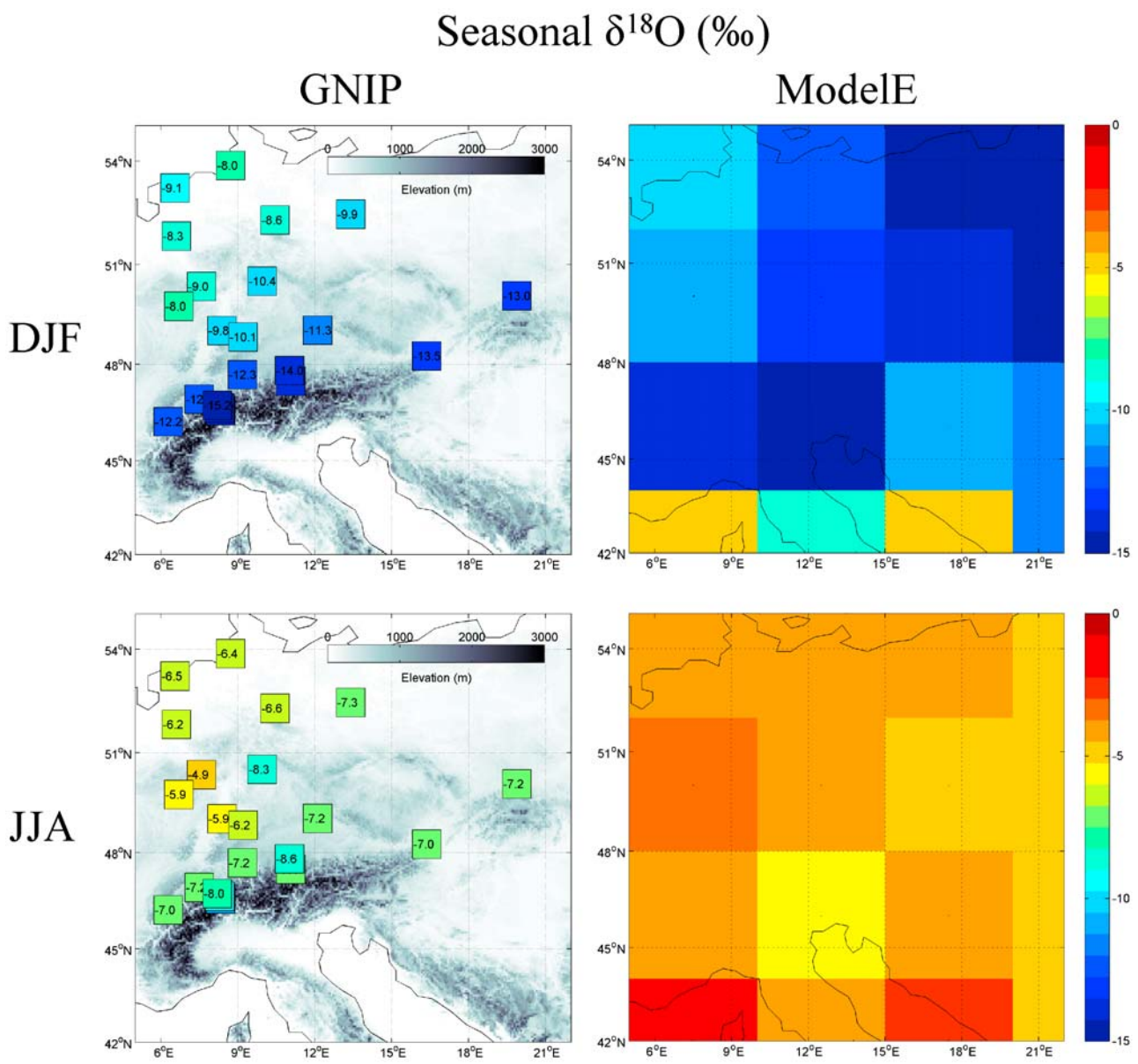

Figure 4. Seasonal precipitation δ^{18}O (‰) at GNIP stations (left) and ModelE (right).

3.4. Atmospheric Circulation Controls on δ^{18}O

[17] The spatial extent and multicentered structure of temperature-δ^{18}O correlations in Figure 7 suggests the influence of broad, circulation controls on δ^{18}O. Following *Baldini et al.* [2008], Figure 8 shows the correlation between the NAO index [*Jones et al.*, 1997] and the monthly δ^{18}O anomalies at each station, for different seasons. There were pronounced correlations during DJF between NAO and δ^{18}O anomalies, with maximum and median correlations across stations of $r = 0.77$ and $r = 0.37$, respectively. Statistically significant correlations were largely absent during JJA, with a maximum of only $r = 0.32$ and a median of $r = 0.15$. Of particular significance is the absence of significant positive correlation across the high-elevation sites in the Alps, where significant temperature correlations were found even during JJA. This suggests more local, exclusively orographic mechanisms for the JJA temperature effect in the Alps, or, if one should exist, a dominant circulation control other than the NAO. Similar seasonal changes were seen for NAO and regional δ^{18}O compared to individual stations. With all months, there was a correlation of $r = 0.34$ between the NAO and regional δ^{18}O, with correlations of $r = 0.56$ during DJF and $r = 0.21$ for JJA. This lower summer correlation likely reflects the absence of any NAO influence on the alpine locations, in contrast to the temperature effects present at the alpine sites during the summer.

[18] It is unsurprising that such relationships exist, given that the NAO significantly influences climate over Europe [*Hurrell et al.*, 2003]. There is no a priori reason why the NAO need be *the* dominant circulation control over European precipitation δ^{18}O, however, given the complex set of factors that influence precipitation δ^{18}O. It is possible that other, distinct, circulation features more strongly influence Euro-

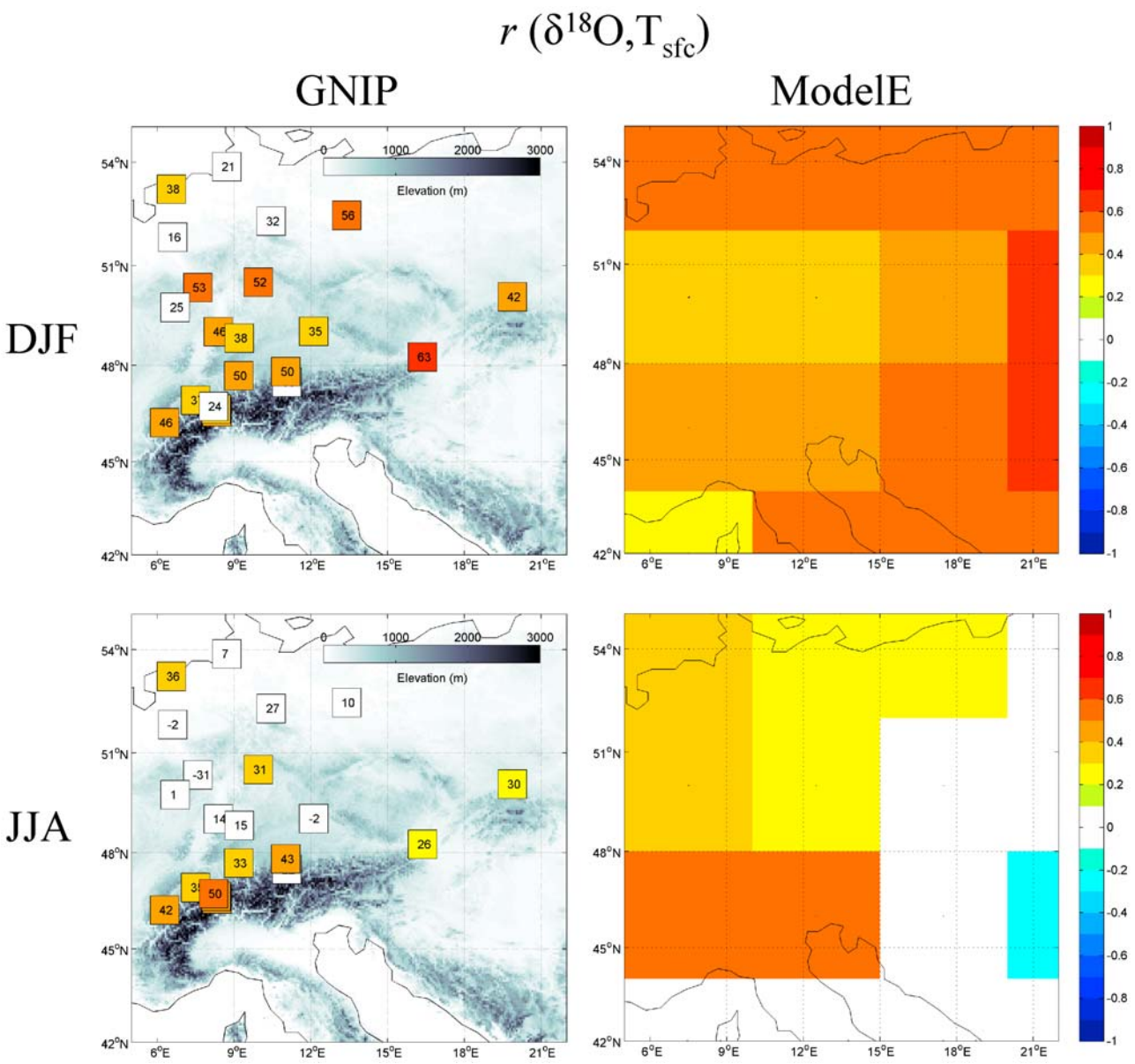

Figure 5. Correlation between monthly temperature and precipitation δ^{18}O anomalies for GNIP stations (left) and ModelE (right). Numbers in GNIP boxes are $r \times 100$. White shading indicate $p > 0.05$. GNIP correlations are for 1963–2001, with the record for each station varying within that period.

pean precipitation δ^{18}O than the NAO. To assess whether this was the case, correlation maps were constructed between regional European δ^{18}O and various meteorological fields characterizing atmospheric circulation, similar to previous studies of δ^{18}O controls over the Greenland and Antarctica [*Werner and Heimann*, 2002; *Schmidt et al.*, 2007], the southwest Yukon [*Field et al.*, 2010], and low-latitude ice core sites [*Vuille and Werner*, 2005; *Vuille et al.*, 2005].

[19] Figure 9 shows correlation maps between monthly anomalies of the regional European δ^{18}O and spatial fields of sea level pressure (SLP) and surface winds. During DJF, there were clear circulation controls over GNIP δ^{18}O, characterized by a north-south dipole centered over the analysis region. The dipole was NAO-like but with centers of action different than in standard definitions, a point which is discussed below. The center of the negative correlation pole had a minimum correlation of $r = -0.58$ and was centered over eastern Scandinavia, arcing from Iceland to central Asia, and the center of positive correlation had a magnitude of $r = 0.72$ and was located over the central Mediterranean Sea. Thus, less-depleted δ^{18}O over Europe is associated with a broad low-pressure anomaly to the north and a high-pressure anomaly to the south. Associated with the SLP dipole were pronounced controls in surface flow indicated by the correlation vectors. There was a positive correlation between δ^{18}O and southwesterly flow into the region, which formed part of the anticyclonic flow around the positive center and cyclonic flow around the negative center.

[20] This dipole structure was well captured in the GCM. The center of the negative correlation region was over the Norwegian Sea, west of that in the observations, but with the same arc stretching from Iceland to Central Asia with a

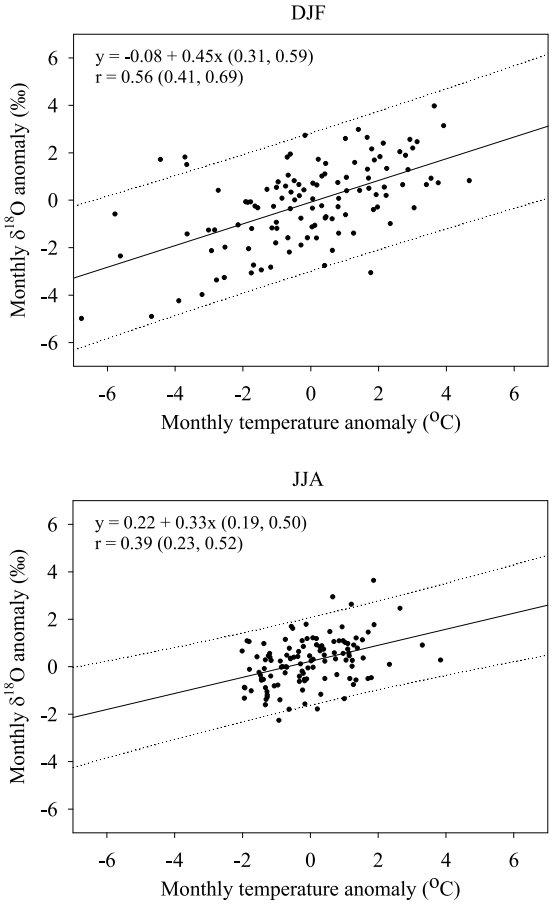

Figure 6. Regionally averaged temperature and δ^{18}O anomalies over central European GNIP stations, with estimated line of best fit and 95% prediction intervals. Equations show estimated line of best fit parameters with 95% bootstrap confidence intervals for slope and correlation in parentheses.

minimum correlation of $r = -0.67$. The main positive correlation center was located in an identical position over the Mediterranean as for observations, with a maximum correlation of $r = 0.69$. The southwesterly flow into the analysis region was also apparent, along with the cyclonic and anticyclonic flow around the negative and positive correlation centers, respectively. In both observations and the GCM, there were also correlation centers appearing outside of the European sector, with negative correlation over much of the Arctic and extending into Canada and positive correlation centers over Bermuda and Hawaii.

[21] Like in the temperature controls, there were weaker circulation controls during JJA. The maximum positive SLP correlation over the Mediterranean, for example, dropped to $r = 0.38$ and $r = 0.36$ for observations and GCM, respectively, with the signatures of all DJF correlation patterns contracting. Correlation maps were also constructed for all months of the year (not shown) and, as for temperature (Figure 7), were simply weakened versions of the DJF correlation maps.

[22] Anomaly correlation maps were also constructed between European precipitation δ^{18}O and geopotential height at 500 hPa (Z_{500}) to identify any possible midtropospheric controls on δ^{18}O (Figure 10). During DJF, the main center of positive Z_{500} correlation in the observations was centered identically to that in the SLP fields, with a maximum correlation of $r = 0.75$. The region of negative correlation was centered in the high north Atlantic and had a more wavelike quality than the SLP correlation field, arcing around the positive correlation center to North Africa. The positive correlation centers over the Bermuda and Hawaiian subtropical highs seen in the SLP correlations were also apparent in the Z_{500} correlations, and there were new positive correlation centers over the Arabian Sea and Siberia, the latter of which could be linked with the Hawaiian correlation center. These features also appeared in the GCM, where the negative correlation center also arced around the Mediterranean but with a greater concentration over the North Atlantic and also with the positive correlation centers in the subtropics and Siberia. In both the observations and GCM, controls were characteristically weaker in JJA but still with moderate positive correlation centers over the Mediterranean and negative correlation centers over the north Atlantic.

[23] All surface and midtropospheric δ^{18}O correlations are summarized in Table 2, with selected correlations plotted in Figure 11 with 95% CIs. Following the Azores-Iceland definition of the station-based NAO index, correlations were also calculated for a simple index based on the difference in SLP at the locations with maximum and minimum correlations. When the uncertainty in the estimator is considered, there is overlap in the range of the local (T_{local}) and regional maximum temperature (T_{regional}) correlations for observations, but greater separation in the GCM (Figure 11). Circulationwise, there was a more robust separation between the NAO index and the controls identified emprically from the SLP and Z_{500} and fields. Overall, the strongest and best-separated controls were at the center of the positive Z_{500} correlation region ($Z_{500\text{max}}$) and the SLP difference index (SLP_{diff}), both of which were consistently outside of the NAO correlation's 95% CI. This was followed by the maximum regional temperature. In general, correlations were higher during DJF than JJA and also better constrained in terms of their confidence interval width. In most cases, correlations from the GCM were stronger than observed correlations but not outside of the latter's confidence intervals.

4. Discussion

4.1. Temperature Controls

[24] The local temperature-δ^{18}O correlations over Europe identified here have been well observed in previous observational studies [*Rozanski et al.*, 1992] and consistently identified at midlatitudes in GCM simulations [*Hoffmann et al.*, 1998; *Cole et al.*, 1999; *Noone and Simmonds*, 2002; *Schmidt et al.*, 2007]. The correlations computed from the GNIP observations were weaker than previous studies which was due to the use here of monthly anomalies in place of December, January, February, and March averages [*Baldini et al.*, 2008] and without the smoothing of *Rozanksi et al.* [1992].

[25] There were significant regional and seasonal variations in the temperature-δ^{18}O correlations computed across Europe. In general, annual temperature-δ^{18}O correlations (not shown) were the combination of a strong winter pattern and a weak summer pattern (Figure 5), with the exception of the Alpine regions, where strong summer correlations persisted, and further inland at Vienna and Krakow, where weaker, but statistically significant correlations persisted. The

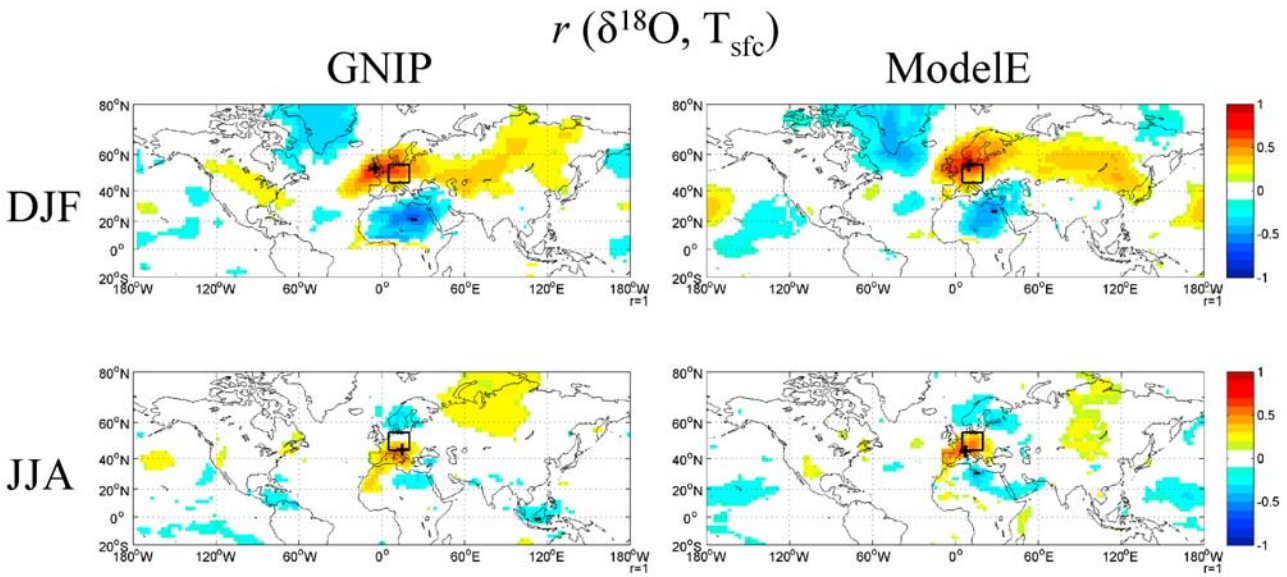

Figure 7. Correlation between European δ^{18}O (in the black rectangle) and surface temperature for GNIP/Reanalysis (left) and ModelE (right). Only correlations significant at the 95% level are shown. The "+" sign indicates the location of maximum positive correlation, and the "–" sign indicates the location of minimum negative correlation.

presence of JJA correlations in these regions is likely due to Rayleigh depletion, in the Alps due to the orographic "altitude effect" [*Araguas-Araguas et al.*, 2000; *Gat*, 2000], and in Vienna and Krakow due to their location further away from the Atlantic ocean, considered the dominant moisture source over central Europe [*Rozanski et al.*, 1982; *Numaguti*, 1999].

[26] The weaker JJA temperature-δ^{18}O correlations are well-known at midlatitudes and have been attributed almost universally to the influence of evapotranspiration, which acts as a nonfractionating moisture source that obscures the depleting effects of Rayleigh distillation [*Jacob and Sonntag*, 1991; *Fricke and O'Neil*, 1999; *Kurita et al.*, 2004; *Peng et al.*, 2004; *Lee et al.*, 2007]. Estimates of moisture recycling vary depending on the data and approach used, but over Europe, consistently show a significant increase in the ratio of moisture recycled over land during summer compared to winter [*Dirmeyer and Brubaker*, 2007]. This is likely an important contributor to the more enriched summer δ^{18}O over Europe and to the weakened temperature-δ^{18}O correlations seen here. Related to this, it is also possible that within-atmosphere post condensation exchange between precipitation and vapor modifies or even erases initial δ^{18}O signatures [*Gat*, 2000; *Worden et al.*, 2007], particularly for liquid phase precipitation which will be prevalent during the summer and lends itself more strongly to condensate-vapor exchange than solid phase precipitation [*Friedman et al.*, 2002]. Statistically, the effect of these two processes is to reduce the variability of precipitation δ^{18}O during the summer. This can be seen in Figure 6, where the ranges of temperature and δ^{18}O anomalies are much smaller during JJA than DJF, contributing to the weaker JJA correlation.

[27] The GCM captured the basic range and seasonality of temperature-δ^{18}O correlations across Europe but did only a modest job of capturing their spatial variation. This agreement in the overall range but disagreement in the spatial pattern between model and observations over Europe is similar to previous GCM results [*Hoffmann et al.*, 1998; *Noone and Simmonds*, 2002]. During DJF, the correlations over Germany were underestimated by the GCM, which, conversely, seemed to overestimate the temperature effect further inland. During JJA, the GCM overestimated the temperature correlations over Germany and underestimated them further inland. A possible factor for this difference is the GCM's JJA bias toward less depleted δ^{18}O seen in Figure 4. This warm summer bias was observed in more detail for the entire annual cycles in Groningen and Vienna [*Schmidt et al.*, 2005] and is likely related to the GCM's ~3°C summer JJA bias over Europe, seen in a more comprehensive model-observation comparison [*Schmidt et al.*, 2006]. One feature that was captured, despite the GCM's low topographic resolution, was the persistent JJA temperature correlation over the Alps. While care should be taken in interpreting GCM results over that small a region, this does illustrate the GCM's ability to capture isotopic relationships over regions with a single strong control, in this case orographic rainout, which is consistent with the absence of strong NAO controls over the Alps during JJA.

[28] These local temperature correlations were part of a broader pattern of positive temperature correlation (Figure 7), which was better captured by the GCM than the within-Europe variation in controls. The positive correlation centers extending outside of Europe reflect a Rayleigh-like temperature control over condensation and δ^{18}O distillation and also, more simply, the spatial covariation of temperature at synoptic scales. This covariation was exclusively the case for the negative correlation centers positioned over eastern North Africa, weaker downstream positive correlation center over Siberia, and weak upstream negative correlation center over Greenland. *Werner and Heimann* [2002] identified a positive temperature correlation pattern over central Greenland δ^{18}O,

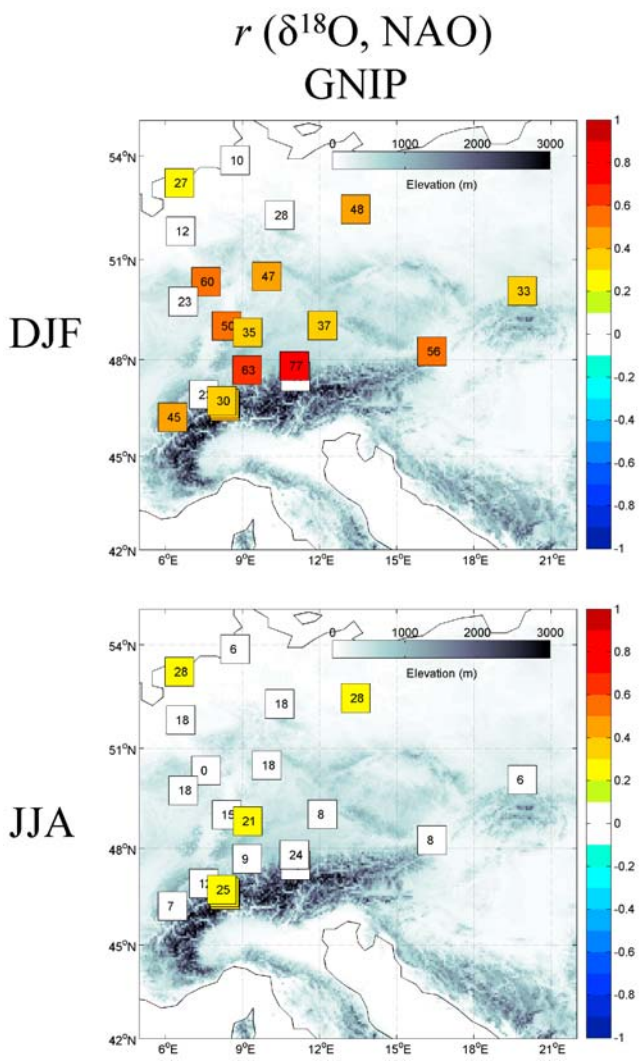

Figure 8. Correlations between the NAO index [*Jones et al.*, 1997] and monthly anomalies of δ^{18}O at GNIP stations, for different seasons. Numbers in GNIP boxes are $r \times 100$. White shading indicate $p > 0.05$.

but not as part of a multicentered teleconnection like that seen here. That study considered annual δ^{18}O, however, and broad temperature patterns associated with Greenland δ^{18}O might be identified with seasonal separation.

4.2. Circulation Controls

[29] Following *Baldini et al.* [2008], a strong NAO control on δ^{18}O was identified during DJF (Figure 8), and the analysis here helped to elucidate its physical structure. The strength of the surface circulation controls was comparable to that of regional temperature and was in fact stronger than local temperature in both observations and the GCM. The correlation vectors at the surface (Figure 9) also help to explain the temperature-δ^{18}O correlations in Figure 7. Less depleted δ^{18}O was associated with enhanced southwesterly flow to the north of the analysis region, representing a northward shift in the storm track and anticyclonic flow around the Mediterranean high. The stronger southerly component to the flow into the analysis region itself would be associated with warmer temperatures, and less moisture distillation, resulting in less depleted δ^{18}O during precipitation events over central Europe. An additional factor could be that the moisture is coming from more proximate sources than when transported over the high North Atlantic and therefore undergoes less Rayleigh depletion during transport. The circulation controls also help to explain the strong dipole in temperature correlations in Figure 7. The elevated δ^{18}O values over Europe were associated with cooler temperatures over North Africa, which, in turn, were associated with stronger northerly flow to the east of the Mediterranean center of positive correlation (Figure 9).

[30] Despite the uncertainty in the estimated correlations, the strength of the anticyclonic circulation over the Mediterranean was as strong a predictor of European δ^{18}O as regional temperature, which is perhaps surprising given the traditional focus on local temperature as the main extratropical control over δ^{18}O. Although the physical reasons for this require further investigation, this could reflect the fact that circulation variability strongly captures transport pathways, and therefore distillation distance, consistent with the argument of *Schmidt et al.* [2007] that isotopic archives may be better interpreted in a non-local sense.

[31] As was the case for local temperature, atmospheric circulation controls were stronger for DJF than JJA, with the annual controls representing a strong winter signal muted by summertime noise. This is almost universally the case for the extratropical teleconnection patterns themselves, which are stronger during winter than summer, due to enhanced temperature gradients zonally and between land and sea. This certainly applies to the NAO which, although unique among extratropical teleconnection patterns in being present during all seasons, is much stronger in winter than summer [*Hurrell et al.*, 2003]. It is argued that this seasonal difference in circulation controls contributes to the reduced summer variability in, and correlation between, temperature and δ^{18}O over Europe, in addition to the buffering effects of continental moisture recycling.

4.3. Teleconnection Signatures

[32] The teleconnection signatures in the circulation correlation maps corresponded to well-known modes of northern hemisphere (NH) variability. At the surface, the Mediterranean-North Atlantic dipole (Figure 9) was NAO-like, and the distinct correlation centers for the Bermuda and Hawaiian high-pressure systems in the subtropics have also been associated with this leading NH mode of variability [*Wallace and Gutzler*, 1981]. This is also the case for the negative correlation pattern spanning the Arctic and extending over Canada. In combination, the signatures in the correlation maps are in fact similar to those of the Arctic Oscillation (AO) or NAM, a more general mode of NH variability of which the NAO has been described a regional expression [*Thompson and Wallace*, 1998; *Thompson et al.*, 2003]. Further evidence of a more broad NH signature were seen in the midtropospheric circulation controls. The transition from an NAO-like north-south dipole at the surface (Figure 9) to a more wavelike structure in the midtroposphere (Figure 10) is remarkably similar to the same vertical change seen between surface and midtroposphere correlation maps between the geopotential

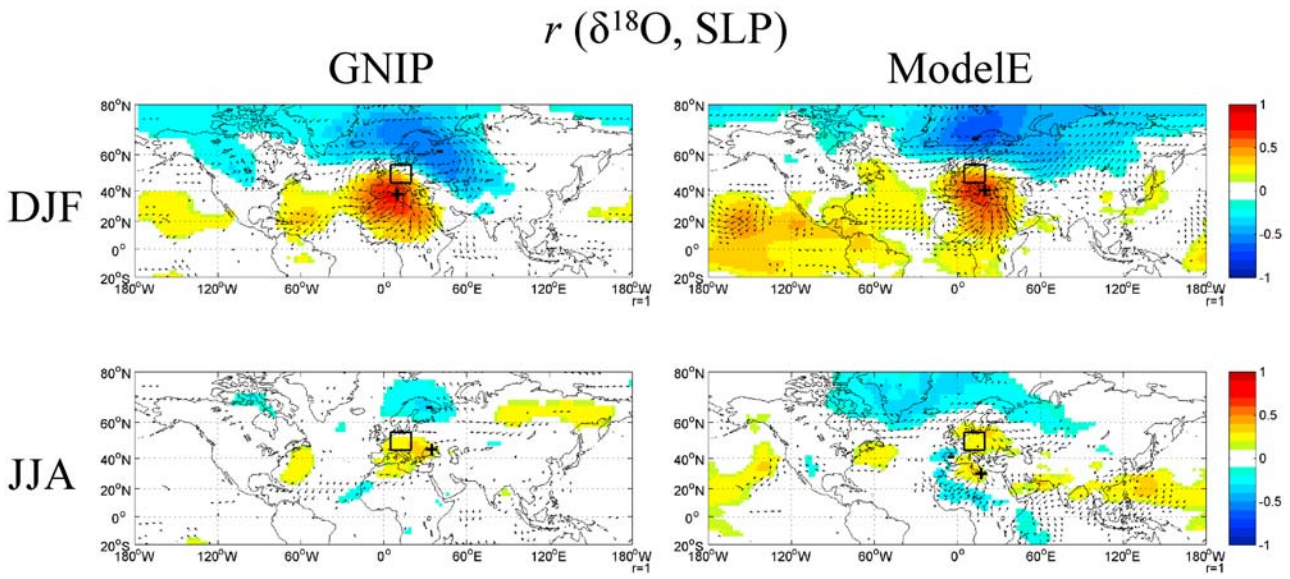

Figure 9. Surface circulation controls over European precipitation δ^{18}O for GNIP/Reanalysis (left) and ModelE (right). The colored shading shows the correlation between monthly anomalies in precipitation δ^{18}O in the boxed region and SLP anomalies. The arrows show the correlation between precipitation δ^{18}O and the **u** and **v** wind components, plotted as a vector.

height and AO/NAM [*Thompson and Wallace*, 1998; *Baldwin and Dunkerton*, 1999]. This is also the case for the midtropospheric emergence of positive correlation centers over Siberia and the Arabian Sea. Remarkably, European δ^{18}O variability would appear to reflect a complete spatial expression of the NAM, extending well beyond the Atlantic sector, which we note in the context of the debate between the NAO or AO/NAM points of view [*Wallace*, 2000].

[33] This analysis focused on the controls over δ^{18}O for a specific region. From the opposite perspective, *Schmidt et al.* [2007] identified the isotopic signature of the NAM by constructing correlation maps between an SLP-based NAM index and precipitation δ^{18}O. In that study, moderate positive correlations were observed across Europe, indicating an association between less depleted δ^{18}O and positive phase of their empirical orthogonal function (EOF)-defined mode. This, in turn, is consistent with the positive phase of the NAO-like dipole in Figure 9. Similarly, *Yoshimura et al.* [2008] considered the isotopic signature of the AO across the northern hemisphere for the GNIP observations and

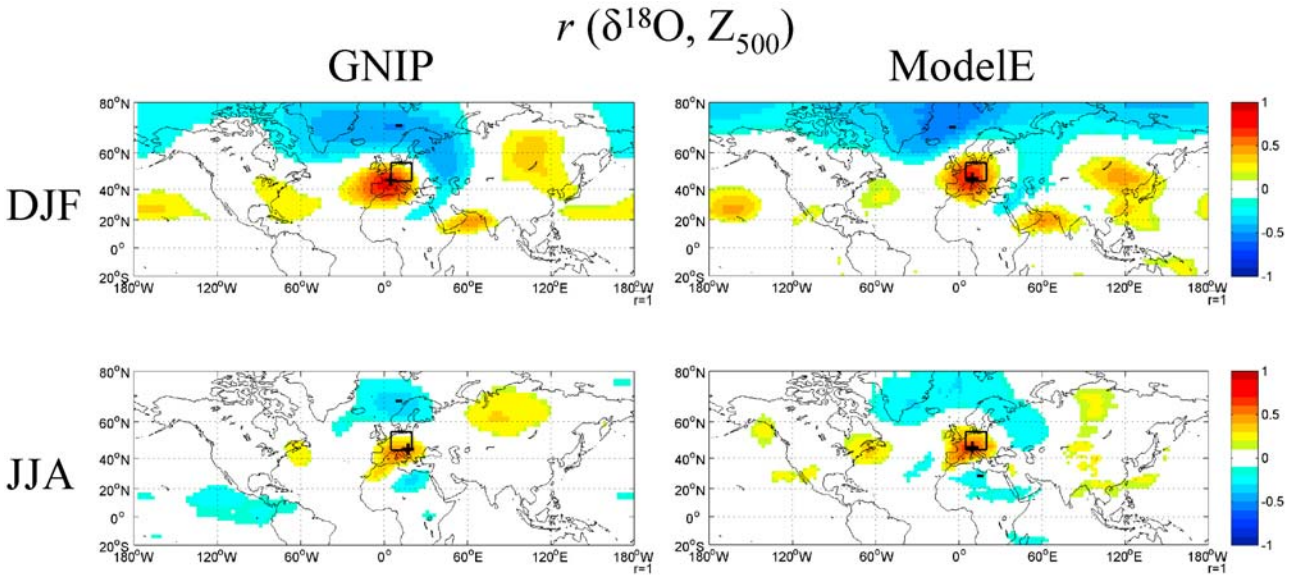

Figure 10. Midtropospheric circulation controls over European precipitation δ^{18}O for GNIP/Reanalysis (left) and ModelE (right). The colored shading shows the correlation between monthly anomalies in precipitation δ^{18}O in the boxed region and Z_{500} anomalies.

Table 2. Correlation Summary for GNIP δ^{18}O Observations and the ModelE GCM[a]

				SLP			Z_{500}	
Months	T_{local}	$T_{regional}$	NAO	Min	Max	Max-min	Min	Max
				GNIP				
All	0.48	0.47	0.34	−0.47	0.55	0.58	−0.40	0.66
DJF	0.57	0.67	0.56	−0.58	0.72	0.72	−0.49	0.75
JJA	0.39	0.51	0.21	−0.32	0.38	0.43	−0.37	0.55
				Model E				
All	0.54	0.56	0.46	−0.52	0.59	0.63	−0.47	0.68
DJF	0.58	0.74	0.59	−0.67	0.69	0.78	−0.58	0.72
JJA	0.43	0.63	0.37	−0.38	0.36	0.52	−0.34	0.64

[a](T_{local}), Local Surface Temperature; ($T^{regional}$), maximum regional surface temperature; NAO based on station observations (NAO_{stn}), NAO based on model data (NAO_{mod}), SLP and Z_{500} at the locations of minimum and maximum correlations and for the difference of the two.

several isotopic GCMs, finding essentially the same signature. In both of these studies, the correlations were comparable to an annual analyses (not shown) and weaker than for our DJF analyses.

[34] Despite the similarities to well-known teleconnection patterns, it should be emphasized that the centers of action in the correlation maps here were different from those in standard definitions. The SLP centers of action in Figure 9, for example, were well to the east of the standard NAO index [*Jones et al.*, 1997], which is based on the difference between SLP over the Azores and Iceland. The EOF-based index by *Trenberth and Paolino* [1980], as described by *Hurrell et al.* [2003], shows a northern center of negative correlation corresponding generally to those identified here but with the southern positive correlation center located well to the west of the positive center over the Mediterranean in Figure 9. Furthermore, no improvements were gained by using the Climate Prediction Center NAO index based on the EOF-based approach of *Barnston and Livezey* [1987].

4.4. Implications for Paleoclimate Reconstruction

[35] The results of this study have implications for traditional interpretations of δ^{18}O based on local temperature, or on hemispheric modes of variability. First, the improvements in considering regionally averaged δ^{18}O from GNIP rather than those at individual stations illustrates the utility of combining multiple, targeted, isotopic archives across a given region. This technique has been applied for Greenland ice cores [*White et al.*, 1997; *Rogers et al.*, 1998] and for tree cellulose [*Treydte et al.*, 2007; *Saurer et al.*, 2008] in reconstructing short-term climatic variability; further δ^{18}O calibration and reconstruction efforts should emphasize this approach. With regional averaging and seasonal separation, less depleted δ^{18}O over Europe was associated with warmer temperatures, more southerly flow, and the positive phase of a hemisphere-wide mode of variability very similar in structure to the NAM. These controls could be considered when interpreting δ^{18}O archives, such as tree ring cellulose and speleothems, which are strongly controlled by precipitation δ^{18}O.

[36] The NAM-like expression was identified through an empirical analysis of the controls rather than with a single circulation index and a priori assumption of the dominant control. Indeed, as *Hurrell et al.* [2003] state, there is no single way of defining the NAO, and in general, isotopic calibrations based on predefined circulation indices may, in a statistical sense, miss their target. The spatial analysis here guards against any sensitivity to one particular definition and illustrates the improvements that can be gained from allowing the controls over a region's δ^{18}O to emerge empirically, and for the possibility of nonlocal controls [*Schmidt et al.*, 2007], which in this case were consistently stronger than the local controls. Further, it has been suggested that future paleoclimatic reconstructions emphasize specific spatial patterns of temperature and atmospheric circulation in place of hemispheric-wide averages, or single circulation indices [*Jones et al.*, 2009], and the controls identified here contribute toward such reconstructions. Isotopic archives in strongly correlated or anticorrelated regions could be combined in a targeted fashion for reconstructions of hemisphere-wide modes of variability, similar to what has been proposed in the tropics for the Andean and Himalayan ice cores [*Schmidt et al.*, 2007]. This could also be used to distinguish periods of hemisphere-wide temperature change from more internally driven reorganizations of circulation, or to examine the temporal stability of a given teleconnection.

[37] There were strong seasonal differences for both observations and the GCM in the temperature and circulation controls, with both being strong in the winter and weak in the summer. This underscores the improvements that can be gained by calibrating isotopic archives for different seasons due to the varying strength of atmospheric circulation controls on precipitation δ^{18}O, in addition to the seasonally vary-

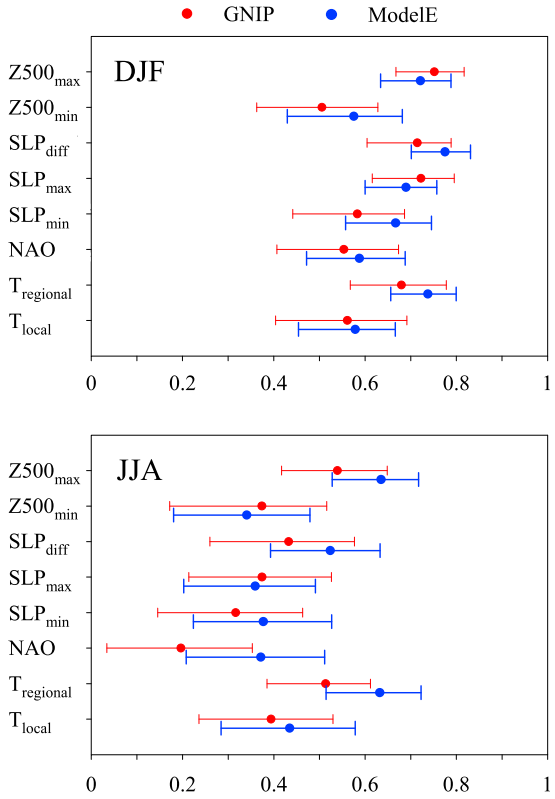

Figure 11. Correlation between precipitation δ^{18}O over Europe and selected variables from Table 2. Error bars are bootstrap-estimated 95% confidence intervals.

ing influence of precipitation δ^{18}O on the particular archive. This is possible with high-resolution sampling for select speleothems [*Mattey et al.*, 2008] and tree rings [*McCarroll and Loader*, 2004], although the more complex fractionation processes in both make climatic interpretation more difficult [*Fairchild et al.*, 2006]. But, conversely, given that subannual resolution will not always be available or summer precipitation δ^{18}O may dominate the archive's signal in the case of tree ring cellulose, the best possible annual controls on δ^{18}O can be identified through the empirical approach used in this study.

5. Conclusions

[38] In this study, an attempt was made to better understand the controls on European precipitation δ^{18}O using GNIP observations and an isotopically equipped GCM, motivated by interests in improving interpretation of paleoclimatic proxies in the region and validating the GCM's ability to identify atmospheric circulation controls. The main findings of this study were as follows:

[39] (1) Stronger temperature and circulation controls were identified for regional European δ^{18}O compared to individual sites, illustrating the potential gains from considering multiple isotopic archives.

[40] (2) Less depleted δ^{18}O over Europe is associated with warmer temperatures, southerly flow, deep anticyclonic circulation over the Mediterranean, and the positive phase of an NAM-like mode of northern hemisphere variability. Statistically, the regional temperature and large-scale circulation controls were stronger than local temperature controls.

[41] (3) The annual controls over δ^{18}O are combinations of strong winter and weak summer controls. In addition to continental moisture recycling, the weaker summer controls are due to reduced variability in the summer circulation.

[42] The GCM performed well in capturing the large-scale controls on European δ^{18}O observed in the GNIP data, most significantly the structure of the NAM through the depth of the troposphere and the weaker controls on δ^{18}O during the summer. In general, the performance of the GCM in capturing these large-scale controls over Europe from observations should give us confidence in using it to identify controls over less data-rich regions at midlatitudes. Also, the GCM could in theory be used to more mechanistically separate underlying controls on δ^{18}O. In future studies, for example, it would be interesting to separate the effects of evapotranspiration and atmospheric moisture recycling from those associated with "pure" Rayleigh distillation and changing circulation through a series of source tagging and sensitivity experiments. The local temperature controls were not as well captured by the GCM due to its coarse resolution, and indeed, GCMs are better suited to studies of large-scale controls on δ^{18}O [*Vuille et al.*, 2005]. It would be worth examining the performance of the isotopically equipped version of the regional circulation model REMO [*Sturm et al.*, 2005] in modeling the variation of local δ^{18}O controls within Europe or elsewhere.

[43] **Acknowledgments.** This work was supported by the Canadian Foundation for Climate and Atmospheric Sciences through the Polar Climate Stability Network and a graduate scholarship from the Natural Sciences and Engineering Research Council of Canada. The author thanks Dylan Jones, Shunli Zhang, Heather Andres and two anonymous reviewers for helpful comments, and acknowledges the availability of GNIP data from the IAEA and the ModelE GCM from NASA GISS.

References

Araguas-Araguas, L., K. Froehlich, and K. Rozanski (2000), Deuterium and oxygen-18 isotope composition of precipitation and atmospheric moisture, *Hydrol. Process.*, *14*(8), 1341–1355.

Baldini, L. M., F. McDermott, A. M. Foley, and J. U. L. Baldini (2008), Spatial variability in the European winter precipitation delta O-18-NAO relationship: Implications for reconstructing NAO-mode climate variability in the Holocene, *Geophys. Res. Lett.*, *35*, L04709, doi:10.1029/2007GL032027.

Baldwin, M. P., and T. J. Dunkerton (1999), Propagation of the Arctic Oscillation from the stratosphere to the troposphere, *J. Geophys. Res.*, *104*(D24), 30,937–30,946.

Barnston, A. G., and R. E. Livezey (1987), Classification, seasonality and persistence of low-frequency atmospheric circulation patterns, *Mon. Weather Rev.*, *115*(6), 1083–1126.

Birks, S. J., and T. W. D. Edwards (2009), Atmospheric circulation controls on precipitation isotope-climate relations in western Canada, *Tellus, Ser. B*, *61*(3), 566–576, doi:10.1111/j.1600-0889.2009.00423.x.

Cole, J. E., D. Rind, R. S. Webb, J. Jouzel, and R. Healy (1999), Climatic controls on interannual variability of precipitation Delta O-18: Simulated influence of temperature, precipitation amount, and vapor source region, *J. Geophys. Res.*, *104*(D12), 14,223–14,235.

Cook, E. R., R. D. D'Arrigo, and M. E. Mann (2002), A well-verified, multiproxy reconstruction of the winter North Atlantic Oscillation index since AD 1400, *J. Clim.*, *15*(13), 1754–1764.

Dirmeyer, P. A., and K. L. Brubaker (2007), Characterization of the global hydrologic cycle from a back-trajectory analysis of atmospheric water vapor, *J. Hydrometeorol.*, *8*(1), 20–37, doi:10.1175/Jhm557.1.

Efron, B., and G. Gong (1983), A Leisurely Look at the Bootstrap, the Jackknife, and Cross-Validation, *Am. Stat.*, *37*(1), 36–48.

Fairchild, I. J., C. L. Smith, A. Baker, L. Fuller, C. Spotl, D. Mattey, F. McDermott, and Eimp (2006), Modification and preservation of environmental signals in speleothems, *Earth Sci. Rev.*, *75*(1–4), 105–153, doi:10.1016/j.earscirev.2005.08.003.

Field, R. D., G. W. K. Moore, G. Holdsworth, and G. A. Schmidt (2010), A GCM-based analysis of circulation controls on δ^{18}O in the southwest Yukon, Canada: Implications for climate reconstructions in the region, *Geophys. Res. Lett.*, *37*, L05706, doi:10.1029/2009GL041408.

Fricke, H. C., and J. R. O'Neil (1999), The Correlation Between O-18/O-16 Ratios of Meteoric Water and Surface Temperature: Its Use in Investigating Terrestrial Climate Change Over Geologic Time, *Earth Plan. Sci. Lett.*, *170*(3), 181–196.

Friedman, I., J. M. Harris, G. I. Smith, and C. A. Johnson (2002), Stable isotope composition of waters in the Great Basin, United States—1. Air-mass trajectories, *J. Geophys. Res.*, *107*(D19), 4400, doi:10.1029/2001JD000565.

Gat, J. R. (2000), Atmospheric water balance—the isotopic perspective, *Hydrol. Process.*, *14*(8), 1357–1369.

Hoffmann, G., M. Werner, and M. Heimann (1998), Water Isotope Module of the ECHAM Atmospheric General Circulation Model: a Study on Timescales From Days to Several Years, *J. Geophys. Res.*, *103*(D14), 16871–16896.

Hurrell, J. W., Y. Kushnir, G. Ottersen, and M. visbeck (2003), An overview of the North Atlantic Oscillation, in *The North Atlantic Oscillation: Climatic Signficance and Environmental Impact*, edited by J. W. Hurrell, pp. 1–36, AGU, Washington, D. C.

IAEA (2001), GNIP maps and animations, edited, International Atomic Energy Agency, Vienna.

Jacob, H., and C. Sonntag (1991), An 8-year record of the seasonal-variation of H-2 and O-18 in atmospheric water-vapor and precipitation at Heidelberg, Germany, *Tellus, Ser. B*, *43*(3), 291–300.

Jones, P. D., et al. (2009), High-resolution palaeoclimatology of the last millennium: a review of current status and future prospects, *Holocene*, *19*(1), 3–49, doi:10.1177/0959683608098952.

Jones, P. D., T. Jonsson, and D. Wheeler (1997), Extension to the North Atlantic Oscillation using early instrumental pressure observations from Gibraltar and south-west Iceland, *Int. J. Climatol.*, *17*(13), 1433–1450.

Jouzel, J., et al. (1997), Validity of the temperature reconstruction from water isotopes in ice cores, *J. Geophys. Res.*, *102*(C12), 26,471–26,487.

Kalnay, E., et al. (1996), The NCEP/NCAR 40-Year Reanalysis Project, *Bull. Am. Meteorol. Soc.*, *77*(3), 437–471.

Kurita, N., N. Yoshida, G. Inoue, and E. A. Chayanova (2004), Modern isotope climatology of Russia: A first assessment, *J. Geophys. Res.*, *109*, D03102, doi:10.1029/2003JD003404.

Lachniet, M. S. (2009), Climatic and environmental controls on speleothem oxygen-isotope values, *Quat. Sci. Rev.*, *28*(5–6), 412–432, doi:10.1016/j.quascirev.2008.10.021.

Lee, J. E., I. Fung, D. J. DePaolo, and C. C. Henning (2007), Analysis of the global distribution of water isotopes using the NCAR atmospheric general circulation model, *J. Geophys. Res.*, *112*, D16306, doi:10.1029/2006JD007657.

Leng, M. J., and J. D. Marshall (2004), Palaeoclimate interpretation of stable isotope data from lake sediment archives, *Quat. Sci. Rev.*, *23*(7–8), 811–831, doi:10.1016/j.quascirev.2003.06.012.

Mattey, D., D. Lowry, J. Duffet, R. Fisher, E. Hodge, and S. Frisia (2008), A 53 year seasonally resolved oxygen and carbon isotope record from a modem Gibraltar speleothem: Reconstructed drip water and relationship to local precipitation, *Earth Planet. Sci. Lett.*, *269*(1–2), 80–95, doi:10.1016/j.epsl.2008.01.051.

McCarroll, D., and N. J. Loader (2004), Stable isotopes in tree rings, *Quat. Sci. Rev.*, *23*(7–8), 771–801, doi:10.1016/j.quascirev.2003.06.017.

McDermott, F. (2004), Palaeo-climate reconstruction from stable isotope variations in speleothems: a review, *Quat. Sci. Rev.*, *23*(7–8), 901–918, doi:10.1016/j.quascirev.2003.06.021.

Noone, D., and I. Simmonds (2002), Associations Between Delta O-18 of Water and Climate Parameters in a Simulation of Atmospheric Circulation for 1979-95, *J. Clim.*, *15*(22), 3150–3169.

Numaguti, A. (1999), Origin and recycling processes of precipitating water over the Eurasian continent: Experiments using an atmospheric general circulation model, *J. Geophys. Res.*, *104*(D2), 1957–1972.

Peng, H. D., B. Mayer, S. Harris, and H. R. Krouse (2004), A 10-yr record of stable isotope ratios of hydrogen and oxygen in precipitation at Calgary, Alberta, Canada, *Tellus, Ser. B*, *56*(2), 147–159.

Proctor, C. J., A. Baker, W. L. Barnes, and R. A. Gilmour (2000), A thousand year speleothem proxy record of North Atlantic climate from Scotland, *Clim. Dyn.*, *16*(10–11), 815–820.

Rayner, N. A., D. E. Parker, E. B. Horton, C. K. Folland, L. V. Alexander, D. P. Rowell, E. C. Kent, and A. Kaplan (2003), Global analyses of sea surface temperature, sea ice, and night marine air temperature since the late nineteenth century, *J. Geophys. Res.*, *108*(D14), 4407, doi:10.1029/2002JD002670.

Rogers, J. C., J. F. Bolzan, and V. A. Pohjola (1998), Atmospheric circulation variability associated with shallow-core seasonal isotopic extremes near Summit, Greenland, *J. Geophys. Res.*, *103*(D10), 11205–11219.

Rozanski, K., C. Sonntag, and K. O. Munnich (1982), Factors controlling stable isotope composition of European precipitation, *Tellus*, *34*(2), 142–150.

Rozanski, K., L. Araguas-Araguas, and R. Gonfiantini (1992), Relation between long-term trends of O-18 isotope composition of precipitation and climate, *Science*, *258*(5084), 981–985.

Saurer, M., P. Cherubini, C. E. Reynolds-Henne, K. S. Treydte, W. T. Anderson, and R. T. W. Siegwolf (2008), An investigation of the common signal in tree ring stable isotope chronologies at temperate sites, *J. Geophys. Res.*, *113*, G04035, doi:10.1029/2008JG000689.

Schmidt, G. A., A. N. LeGrande, and G. Hoffmann (2007), Water isotope expressions of intrinsic and forced variability in a coupled ocean-atmosphere model, *J. Geophys. Res.*, *112*, D10103, doi:10.1029/2006JD007781.

Schmidt, G. A., et al. (2006), Present-day atmospheric simulations using GISS ModelE: Comparison to in situ, satellite, and reanalysis data, *J. Clim.*, *19*(2), 153–192.

Schmidt, G. A., G. Hoffmann, D. T. Shindell, and Y. Y. Hu (2005), Modeling atmospheric stable water isotopes and the potential for constraining cloud processes and stratosphere-troposphere water exchange, *J. Geophys. Res.*, *110*, D21314, doi:10.1029/2005JD005790.

Sonntag, C., and H. Schoch-Fischer (1985), Deuterium and oxygen 18 in water vapour and precipitation: Application to atmospheric water vapour transport and to paleoclimate, *Isot. Environ. Health Stud.*, *21*(6), 193–198.

Sturm, K., G. Hoffmann, B. Langmann, and W. Stichler (2005), Simulation of Delta O-18 in precipitation by the regional circulation model REMOiso, *Hydrol. Process.*, *19*(17), 3425–3444.

Thompson, D. W. J., and J. M. Wallace (1998), The Arctic Oscillation Signature in the Wintertime Geopotential Height and Temperature Fields, *Geophys. Res. Lett.*, *25*(9), 1297–1300.

Thompson, D. W. J., S. Lee, and M. P. Baldwin (2003), Atmospheric Processes Governing the Northern Hemisphere Annular Mode/North Atlantic Oscillation, in *The North Atlantic Oscillation: Climatic Signficance and Environmental Impact*, edited by J. W. Hurrell, pp. 81–112, AGU, Washington, D. C.

Trenberth, K. E., and D. A. Paolino (1980), The Northern Hemisphere sea-level pressure data set—trends, errors and discontinuities, *Mon. Weather Rev.*, *108*(7), 855–872.

Treydte, K., et al. (2007), Signal strength and climate calibration of a European tree-ring isotope network, *Geophys. Res. Lett.*, *34*, L24302, doi:10.1029/2007GL031106.

Trouet, V., J. Esper, N. E. Graham, A. Baker, J. D. Scourse, and D. C. Frank (2009), Persistent positive North Atlantic Oscillation mode dominated the medieval climate anomaly, *Science*, *324*(5923), 78–80, doi:10.1126/science.1166349.

Vinther, B. M., S. J. Johnsen, K. K. Andersen, H. B. Clausen, and A. W. Hansen (2003), NAO signal recorded in the stable isotopes of Greenland ice cores, *Geophys. Res. Lett.*, *30*(7), 1387, doi:10.1029/2002GL016193.

Vuille, M., R. S. Bradley, M. Werner, R. Healy, and F. Keimig (2003), Modeling delta O-18 in precipitation over the tropical Americas: 1. Interannual variability and climatic controls, *J. Geophys. Res.*, *108*(D6), 4174, doi:10.1029/2001JD002038.

Vuille, M., and M. Werner (2005), Stable isotopes in precipitation recording South American summer monsoon and ENSO variability: observations and model results, *Clim. Dyn.*, *25*(4), 401–413, doi:10.1007/s00382-005-0049-9.

Vuille, M., M. Werner, R. S. Bradley, and F. Keimig (2005), Stable isotopes in precipitation in the Asian monsoon region, *J. Geophys. Res.*, *110*, D23108, doi:10.1029/2005JD006022.

Wallace, J. M. (2000), North Atlantic Oscillation/annular mode: Two paradigms—one phenomenon, *Q. J. R. Meteorol. Soc.*, *126*(564), 791–805.

Wallace, J. M., and D. S. Gutzler (1981), Teleconnections in the Geopotential Height Field During the Northern Hemisphere Winter, *Mon. Weather Rev.*, *109*(4), 784–812.

Werner, M., and M. Heimann (2002), Modeling interannual variability of water isotopes in Greenland and Antarctica, *J. Geophys. Res.*, *107*(D1), 4001, doi:10.1029/2001JD900253.

White, J. W. C., L. K. Barlow, D. Fisher, P. Grootes, J. Jouzel, S. J. Johnsen, M. Stuiver, and H. Clausen (1997), The climate signal in the stable isotopes of snow from Summit, Greenland: Results of comparisons with modern climate observations, *J. Geophys. Res.*, *102*(C12), 26,425–26,439.

Worden, J., D. Noone, and K. Bowman (2007), Importance of rain evaporation and continental convection in the tropical water cycle, *Nature*, *445*(7127), 528–532.

Yoshimura, K., M. Kanamitsu, D. Noone, and T. Oki (2008), Historical isotopesimulation using Reanalysis atmospheric data, *J. Geophys. Res.*, *113*, D19108, doi:10.1029/2008JD010074.

R. D. Field, Department of Physics, University of Toronto, 60 St. George St., Toronto, Ontario M5S 1A7, Canada. (robert.field@utoronto.ca)